JACS
JOURNAL OF THE AMERICAN CHEMICAL SOCIETY
pubs.acs.org/JACS
Article

Elastic Network of Droplets for Underwater Adhesives

Hyuna Jo and Seunghyun Sim*

Cite This: J. Am. Chem. Soc. 2023, 145, 27022−27029
Read Online
ACCESS | Metrics & More | Article Recommendations | Supporting Information

ABSTRACT: Functionality in biological materials arises from complex hierarchical structures formed through self-assembly processes. Here, we report a kinetically trapped self-assembly of an elastic network of liquid droplets and its utility for tough and fast-acting underwater adhesives. This complex structure was made from a one-pot mixture of scalable small-molecule precursors. Liquid−liquid phase separation accompanied by silanol hydrolysis, condensation, and zwitterionic self-association yields a viscoelastic solid with interconnected liquid droplets. These hierarchical microstructures increase toughness and enable underwater adhesion for a range of substrates, offering a platform for robust adhesives for rapid underwater repair or emergency wound care.

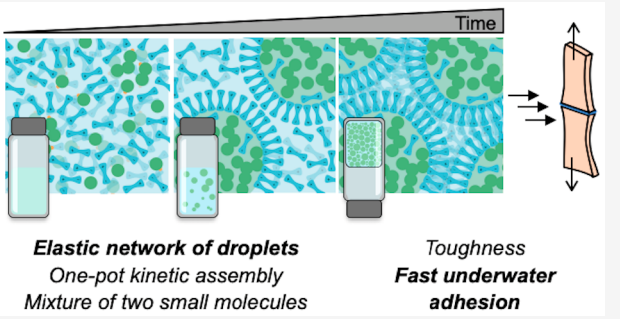

INTRODUCTION

Biology utilizes hierarchical structures under nonequilibrium conditions to program key functions, such as adhesion, transport, and protection.[1−4] Importantly, phase separation of liquid precursors is a powerful mechanism to organize soft and amenable compartments into hierarchical structures in a range of length scales.[5,6] This liquid−liquid phase separation (LLPS) process is driven by various noncovalent intermolecular forces and influenced by multivalent interactions in macromolecules.[7,8] A typical thermodynamic minimum, especially in synthetic systems, is the macroscopic segregation of two phases to minimize the phase boundary (Figure 1a, left). Small droplets growing from nuclei will coalesce into larger ones, and at the end point of LLPS, two distinct macroscopic layers emerge. Interfacial self-assembly to kinetically stabilize synthetic liquid droplets before macroscopic phase segregation has been shown with surfactants, macromolecules, inorganic colloids, and lipid membranes.[9−13]

Efforts to construct macroscopic materials bearing kinetically trapped liquids have been made to recapitulate compartmentalized networks of liquid often found in biological structures, such as tissues (Figure 1a, right). For example, Mann and co-workers reported agarose hydrogels encasing droplets made of double-stranded DNA and dextran by slow cooling the mixture from 60 °C to room temperature.[14] Alternatively, assembling strategies for interface-stabilized droplets have also been demonstrated. Bayley and colleagues showed a method to precisely control the placement and arrangement of lipid-stabilized liquid droplets using microfluidics and 3D droplet printers.[15] Recent work of Qiao and co-workers also demonstrated spontaneous coalescence of polysaccharide-stabilized droplets by centrifugation.[13] Finally, bicontinuous interfacially jammed emulsion gels (Bijel) were made with an emulsifying colloid at the interface between two liquids undergoing spinodal decomposition.[16] Nonequilibrium bicontinuous morphologies are formed by the physical jamming of colloidal particles at the interface between the two liquids. Despite the progress in this area, a scalable method to produce an elastic network of liquids with desirable macroscopic functions is currently lacking.

In this article, we report spontaneous formation of an elastic network of droplets via kinetically trapped self-assembly (Figure 1b). Distinct from previously reported systems incorporating complex liquids within materials (Figure 1a), our system is based on one-pot mixtures of two small-molecule liquid precursors, 3-(trimethoxysilyl)propyl methacrylate (TMeOSMA) and [2-(methacryloyloxy)ethyl]dimethyl-(3-sulfopropyl)ammonium hydroxide (sulfobetaine methacrylate, SBMA), undergoing hydrolysis, condensation, and LLPS at the same time (Figure 1c). Instead of macroscopic phase separation, we observed a spontaneous formation of viscoelastic solids comprising compartmentalized liquid components (Figure 1d). Subsequent polymerization on the methacrylate part of the network demonstrated that this type of hierarchical organization leads to increased toughness, stretchability, and adhesion. Further, we showed that this material functions as photocurable and scalable underwater adhesives for a variety of substrates, including glass, porcine skin, and plastics.

Received: September 23, 2023
Revised: November 9, 2023
Accepted: November 14, 2023
Published: December 4, 2023

https://doi.org/10.1021/jacs.3c10528
J. Am. Chem. Soc. 2023, 145, 27022−27029

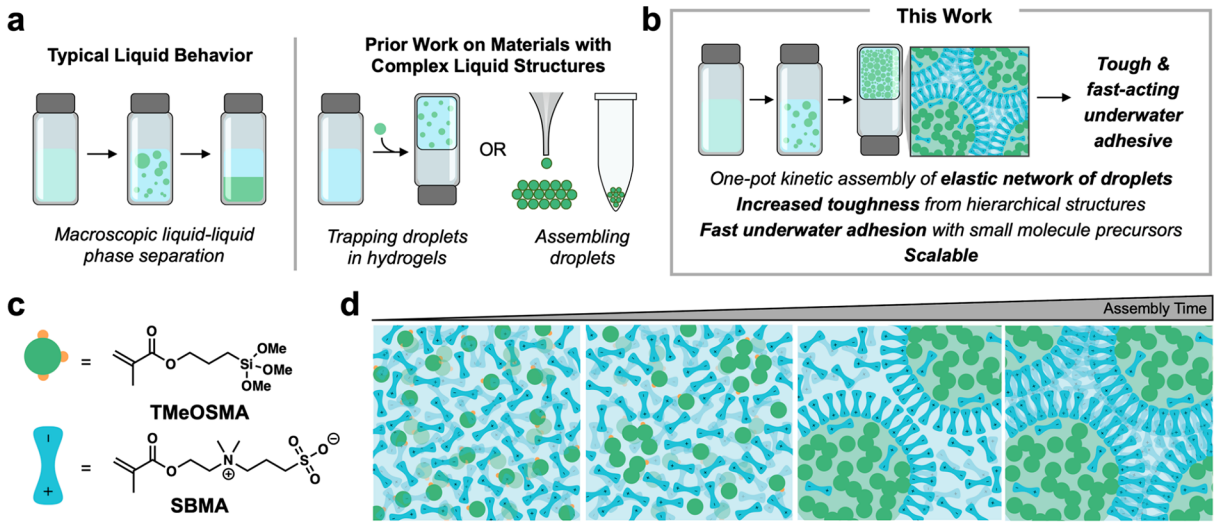

Figure 1. Schematic illustration of this work. (a) Typical LLPS leads to macroscopic segregation of two distinct phases (left). Previous approaches on constructing materials bearing complex liquid structures involve trapping liquid droplets within a hydrogel scaffold or assembling stabilized droplets (right). (b) Summary and features of this work. (c) Chemical structures of the two small-molecule precursors in this study. (d) A schematic illustration of the compartmentalized network formation over time.

RESULTS AND DISCUSSION

Formation of an Elastic Network of Compartments via LLPS. The small-molecule liquid precursors, TMeOSMA and SBMA, are typically immiscible (Figure S3). We serendipitously discovered that bubbling N_2(g) into an aqueous mixture of 0.95 molal concentration (m, solute in mol per solvent in kg) of TMeOSMA and 4.75 m SBMA under acidic conditions (DI water, pH 3) turns the two immiscible phases into one homogeneous phase in 10 min (Supplementary Video 1). Importantly, this mixture does not contain any photoinitiators that may trigger radical polymerization at the methacrylate moiety. This clear solution over time undergoes LLPS characterized by micron-sized compartment formation and increased macroscopic turbidity and after 16 h yields a turbid gel comprising a network of compartments (Figure 2a). The inside of these compartments shows a dark contrast under phase contrast microscopy (Figure 2a), different from typical silica particles showing a bright contrast due to their high refractive index.[17] The same mixture bubbled with air also becomes transparent after 10 min but undergoes macroscopic phase separation within 8 h (Figure S3). Linear rheological measurement of this mixture upon changing assembly time showed a gradual change from viscoelastic liquid to viscoelastic solid, accompanied by orders of magnitude changes in stiffness (Figure 2b).

We hypothesized that relatively more hydrophobic TMeOSMA in an aqueous mixture constitutes a compartment, and zwitterionic SBMA plays the role of surfactant at the interface, similar to surfactant-mediated stabilization of coacervates in prior studies.[10] To test our hypothesis, we conjugated fluorescein amidite (FAM) thiol on each liquid precursor through a Michael addition reaction at the methacrylate part (Figures S1 and S2). FAM-conjugated TMeOSMA (FAM-TMeOSMA) localized inside the compartments (Figure 2c), and FAM-conjugated SBMA (FAM-SBMA) was observed outside and at the boundary of the compartments (Figure 2d), confirming our hypothesis. Based on Jiang and co-workers' previous studies showing that the sulfobetaine motif exhibits an intermolecular zwitterionic self-association (an electrostatic

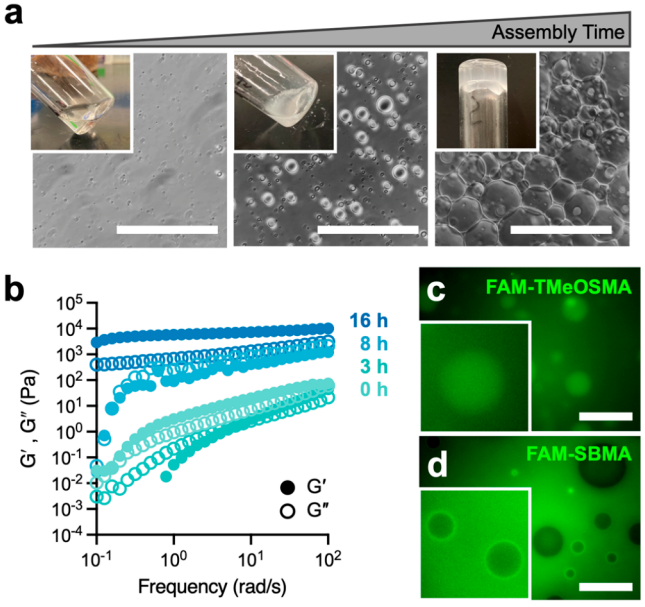

Figure 2. Formation of an elastic network of compartments via LLPS. (a) Representative optical microscopy and photographic images showing the network formation process. Scale bars = 50 μm. (b) Storage moduli G' and loss moduli G'' of the mixture containing SBMA and TMeOSMA over time. (c, d) Fluorescence microscopy (λ_{ex} = 495 nm; λ_{obs} = 690−740 nm) of the mixture containing (c) FAM-TMeOSMA and (d) FAM-SBMA. Images taken at 30 min assembly time after mixing and N_2 bubbling. Scale bars = 20 μm.

locking effect),[18−20] we speculate that SBMA on the compartment surface forms interlocked structures through electrostatic interactions and kinetically stabilizes the network. Similar to typical LLPS, there is an energetic drive for compartments to grow in size, but once the surface SBMA molecules start to form electrostatically interlocked structures, they stop growing. We increased the temperature at which LLPS proceeds to 80 °C and obtained a turbid gel without compartment formation (Figure S7), indicating that the elastic network of compartments is indeed a kinetic product.

https://doi.org/10.1021/jacs.3c10528
J. Am. Chem. Soc. 2023, 145, 27022−27029

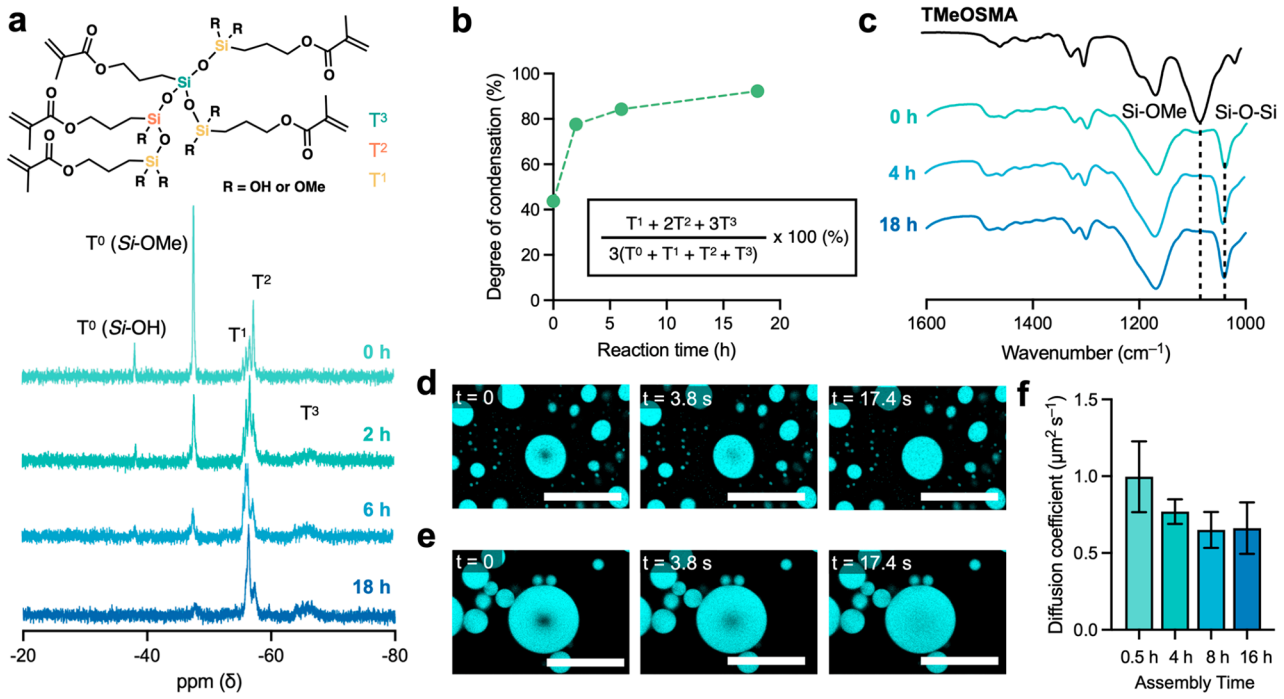

Figure 3. Hydrolysis and silanol condensation occur within liquid droplets. (a) ^{29}Si NMR spectroscopy of the mixture containing TMeOSMA and SBMA over time, and chemical structure illustrating different states of silicon atoms. (b) Degree of condensation (%) of the mixture containing TMeOSMA and SBMA as a function of reaction time. (c) FT-IR spectroscopy of the mixture containing TMeOSMA and SBMA over time. (d, e) Time-lapse confocal laser scanning microscopy images (λ_{ex} = 515 nm; λ_{obs} = 550−630 nm) of the mixture containing Nile red dye (2 μM) at the assembly times of (d) 30 min and (e) 8 h after photobleaching (λ_{ex} = 515 nm, 100% intensity). Scale bars = 30 μm. (f) Diffusion coefficient of the mixture of TMeOSMA and SBMA at different assembly times calculated from the FRAP experiments. Error bars represent ± s.e.m. N = 3.

Hydrolysis and Silanol Condensation Occur within Liquid Droplets. The trimethoxysilyl group from TMeOSMA is known to undergo hydrolysis and condensation reactions under mildly acidic conditions.[21] We hypothesized that upon mixing the two immiscible liquid precursors and bubbling N_2 under acid conditions, hydrolysis of the trimethoxysilyl group into silanol occurs and makes the two liquids miscible, resulting in a homogeneous mixture. ^{29}Si NMR spectroscopy over time revealed dynamic changes in TMeOSMA (Figure 3a). Silicon atoms are labeled with T, and the superscript number represents the number of adjacent siloxane bonds. Even at the beginning of the LLPS process after 10 min of N_2 bubbling (0 h), peaks from the lower degree of the condensed form of silanol (T^1 and T^2) were visible along with a noticeable silanol peak (T^0, Si−OH), indicating that TMeOSMA has gone through acid-mediated hydrolysis and a lower degree of condensation during the N_2 bubbling step. As droplets formed and grew, both the trimethoxysilyl group (T^0, Si−OMe) from the precursor and its hydrolyzed form, silanol (T^0, Si−OH), disappeared. At the same time, peaks from the siloxane oligomers (T^1, T^2, and T^3) gradually increased. The degree of condensation was calculated through the integration of peaks (Figure 3b).[22,23] Condensation rapidly proceeded within the first 2 h and gradually reached up to 95%. We note that despite the high degree of condensation at the end point, most silicon species were at T^1 or T^2. Fourier-transform infrared spectroscopy (FT-IR) of these mixtures also showed that the peak from the Si−OMe stretch started to disappear at the beginning of the LLPS after N_2 bubbling, and a new peak corresponding to siloxane bonds emerged (Figure 3c). Taken together, the SBMA and TMeOSMA mixture becomes miscible upon N_2 bubbling under an acidic condition due to partial hydrolysis of TMeOSMA into silanol, which is more hydrophilic. At the same time, further condensation into macromolecular siloxane triggers LLPS in the course of 16 h.

We then wondered if the internal compartments were indeed liquid droplets. We performed fluorescence recovery after photobleaching (FRAP) experiments to determine the fluidity and diffusion characteristics of the droplets, using Nile red as a probe molecule (Figure 3d−f).[24,25] Upon photobleaching (λ_{ex} = 515 nm, 100% intensity), the fluorescence of droplets recovered up to 70−90% of its initial value in 20 s for all of the time points (Figures S10 and S11). The diffusion coefficients of the dye inside the droplet were determined from the FRAP results (Figure 3f and Figures S10 and S11),[26] revealing a slight decreasing trend in diffusion coefficient as the assembly time increases. Overall, the fluidic nature of the siloxane droplets is maintained through the LLPS process and the resulting elastic network of droplets (END) phase.

Effect of Molecular Structures and Chemical Environment on the END Phase Formation. To test our hypothesis that the electrostatic locking effect of SBMA is responsible for END phase formation, we investigated the effect of molecular structures and compositions on phase behaviors with a few different zwitterionic monomers; SBMA, 3,3-[[2-(methacryloyloxy)ethyl]dimethylammonio]propionate (carboxybetaine methacrylate, CBMA), and 2-methacryloyloxyethyl phosphorylcholine (phosphorylcholine methacrylate, PCMA) (Figure 4a). The ratio of TMeOSMA/zwitterion and total concentrations of small molecules were varied, and the outcomes were recorded based on the macroscopic phases and sol/gel states (Figure 4b and Figure S6). TMeOSMA and SBMA mixtures at low ratios of SBMA resulted in solutions with two macroscopically segregated phases, and at the highest

https://doi.org/10.1021/jacs.3c10528
J. Am. Chem. Soc. 2023, 145, 27022−27029

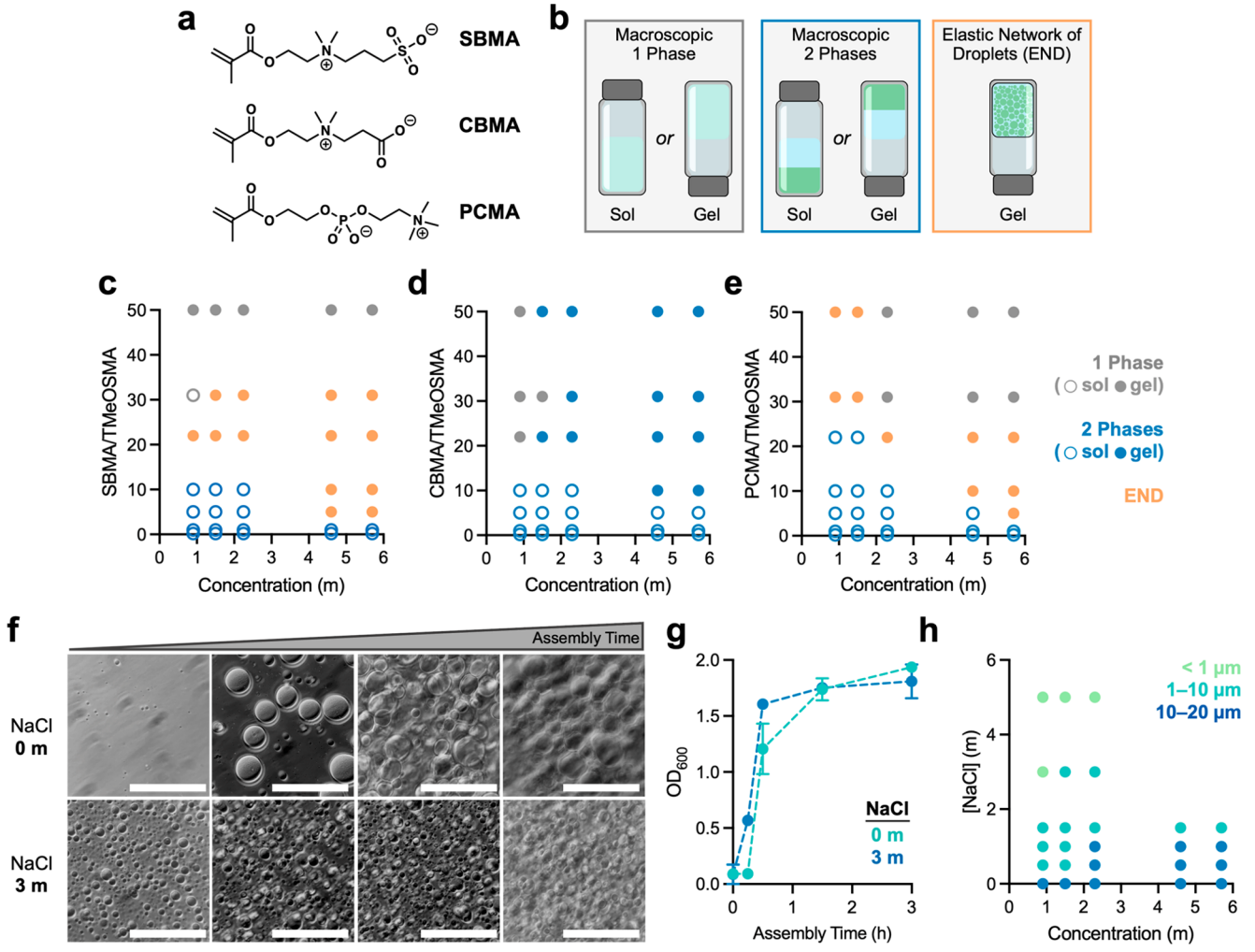

Figure 4. Effect of molecular structures and chemical environment on the END phase formation. (a) The chemical structure of different zwitterions: sulfobetaine methacrylate (SBMA), carboxybetaine methacrylate (CBMA), and phosphorylcholine methacrylate (PCMA). (b) Schematic illustration of the products from mixing TMeOSMA and a zwitterionic precursor. Macroscopic single phase represents a homogeneous mixture (liquid or gel state), and macroscopic double phases represent macroscopic phase segregation of two distinct layers (liquid or gel state). (c–e) Phase diagrams of TMeOSMA mixtures with (c) SBMA, (f) CBMA, and (g) PCMA, varying the total concentration of methacrylate species and zwitterion ratio. (f) Representative optical microscopy images of the mixtures containing SBMA and TMeOSMA in the absence and presence of 3 m NaCl. Scale bars = 50 μm. (g) Absorbance at 600 nm (OD_{600}) of the mixture containing TMeOSMA and SBMA as a function of assembly time. (h) A diagram showing the range of droplet sizes in the mixtures containing SBMA and TMeOSMA. Error bars represent ± s.e.m. N = 3.

ratio of 50, samples with all tested concentrations became macroscopically homogeneous gels in 1 h (Figure 4c). The END phase occurs at the boundary of these two phases. We suspect that when the number of SBMA molecules in a system is not enough to stabilize hydrophobic droplets generated from TMeOSMA, these droplets eventually coalesce into a macroscopic solution. On the other hand, at the highest ratio of SBMA/TMeOSMA, excess SBMA may homogeneously disperse TMeOSMA species and their hydrolyzed forms. A different zwitterionic monomer, CBMA, has been shown to exhibit a lower degree of self-association due to a mismatch in charge density (ammonium cation: 3.0 e/nm^3, sulfate anion: −4.5 e/nm^3, and carboxylate anion: −5.3 e/nm^3).[20] In contrast to the mixtures of SBMA, CBMA mixed with TMeOSMA did not result in the END phase in all tested ratios and concentrations (Figure 4d). Most combinations yielded two macroscopic phases, either in gels or solutions, and the homogeneous single phase was only observed in lower total concentrations and high CBMA ratios. This result highlights the importance of the zwitterion's self-association in arriving at and stabilizing the END phase after the LLPS process. We also tested PCMA, which has been shown to bear a similar charge density to SBMA (ammonium cation: 3.0 e/nm^3, phosphate anion: −3.0 e/nm^3).[20] Similar to SBMA, PCMA and TMeOSMA mixtures yielded the END phase at the phase boundary (Figure 4e, Figure S9).

We also tested whether adding salt, which has been shown to affect electrostatic interactions between charged species,[20,27−29] changes the phase behavior of the system. The mixture of SBMA/TMeOSMA (ratio = 5, total concentration = 5.7 m) in the presence of 3 m NaCl formed smaller droplets than in the absence of NaCl (Figure 4f). Interestingly, in the presence of the salt, droplet formation occurred slightly faster than in the absence of the salt, based on turbidity (OD_{600}) measurements at the early time points (Figure 4g). Both samples arrived at the END phase after 16 h. We also systematically varied the NaCl concentration and the total concentration of the methacrylate species at a fixed monomer

https://doi.org/10.1021/jacs.3c10528
J. Am. Chem. Soc. 2023, 145, 27022−27029

ratio SBMA/TMeOSMA of 5 (Figure 4h and Figure S8). Similar to our observations in Figure 4f, higher concentrations of NaCl result in smaller-sized droplets in all tested concentrations. We were not able to collect data at high concentrations of NaCl and methacrylate species because they yielded precipitation or homogeneous gels (Figure S8). These results show that electrostatic interaction between zwitterionic molecules on the droplet surface determines the energetic landscape and phase behaviors.

Hierarchical Microstructures Increase Toughness and Stretchability. Because the self-assembled droplet mixtures have unreacted methacrylate handles, we set out to study how hierarchical structure impacts the overall mechanical performance of materials. Since the droplet size is a function of NaCl concentration and assembly time (Figure 4f–h), we varied these parameters in our samples. Samples are mixed with a photoinitiator, lithium phenyl-2,4,6-trimethylbenzoylphosphinate (LAP), at various stages of assembly and subjected to photo-cross-linking with 365 nm LED light (Figure 5a). The hierarchical morphology of each state is fixed

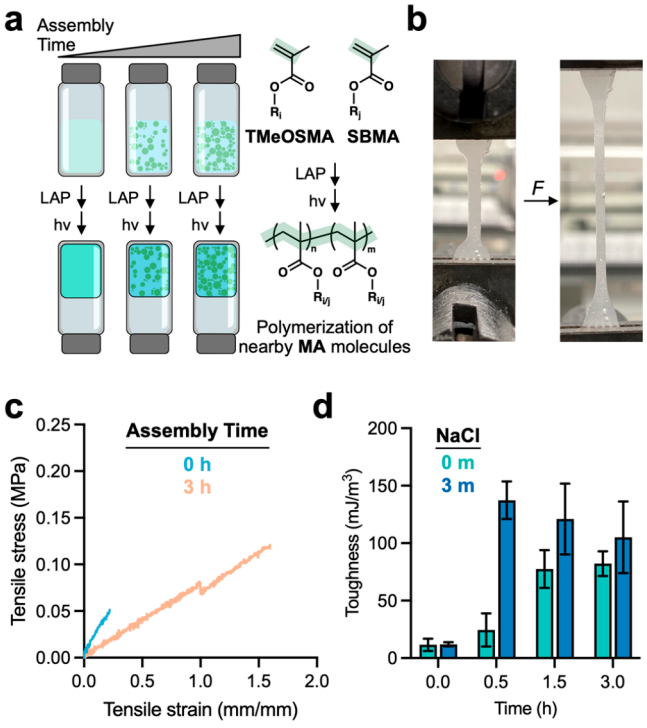

Figure 5. Hierarchical microstructures increase toughness and stretchability. (a) Schematic illustration of the photo-cross-linking process to fix the hierarchical microstructures from LLPS. (b) Representative photographic images of photo-cross-linked samples at 1.5 h assembly time before and after applying axial tensile force. (c) Stress–strain curve of the mixture containing TMeOSMA and SBMA before (0 h) and after (3 h) hierarchical microstructure formation. (d) Toughness of the photo-cross-linked materials with different assembly times and droplet sizes. Error bars represent ± s.e.m. $N = 3$.

by polymerizing the methacrylate part of the two small-molecule precursors. We only compared self-assembled structures within the first 4 h of assembly because introducing LAP to the END phase resulted in heterogeneous material due to the nonhomogeneous incorporation of the photoinitiator and limited light penetration.

Tensile testing of the fixed samples showed that hierarchical microstructures make them less brittle and more stretchable than homogeneous mixtures at the beginning (Figure 5b). There was a clear increase in toughness and failure strain of the materials as the assembly time increased (Figure 5c). Similarly, samples prepared with 3 m NaCl showed an increase in stretchability, toughness, and failure strain with longer assembly time (Figure S12). We systematically varied the assembly time in the absence and presence of 3 m NaCl and compared the resulting materials' toughness (Figure 5d). Mixtures at 0 h without droplet structures yielded brittle materials in both cases. At 0.5 h, the 3 m NaCl mixture with a significant droplet formation showed an 11.4-fold increase in toughness compared to 0 h. The differences in stiffness were correlated with the extent of droplet formation prior to the photopolymerization (Figure 4g). However, we did not observe any obvious effect from the droplet size: When both systems show a similar extent of droplet formation based on turbidity at 3 h assembly time, the stiffness of the resulting materials was similar. Interestingly, longer assembly time also increased macroscopic adhesion to glass substrates, which may have resulted from the structuring of assembled SBMA molecules on the droplet and material surface (Figure S4). To isolate the effect of hierarchical structures from silanol condensation, we prepared photo-cross-linked samples at 0 h and incubated them in an acidic environment for 3 h to promote postcuring silanol condensation. The resulting materials showed increased turbidity but were brittle and exhibited similar mechanical properties to pristine materials cross-linked at 0 h (Figure S13), indicating that hierarchical microstructure is the key to increasing toughness, stretchability, and adhesion of the materials.

Tough and Fast-Acting Underwater Adhesives. Robust adhesion in wet environments is useful for medical and watercraft industries.[30,31] Underwater adhesion is typically more challenging than in air due to the surrounding water molecules.[32−34] Many synthetic underwater adhesives have been developed, but current limitations include impractical curing time (>1 h), use of organic solvents, and multistep synthesis of macromolecules, limiting scalability.[35,36] Encouraged by the observed adhesion and increased toughness of our materials, we investigated their underwater adhesion behavior using various substrates. Briefly, we applied a precursor liquid (300 μL), a mixture that underwent LLPS with a specific assembly time, on the surface of glass, polypropylene (PP), and poly(methyl methacrylate) (PMMA) substrates (10 × 20 mm^2). After placing another substrate directly onto this area, we applied UV irradiation (λ = 365 nm) for 2 min (Figure 6a, upper panel, Figure S25). For testing porcine skin substrates, the precursor mixture was applied to the cross-sectional side (1.5 × 20 mm^2) cut by a razor with the help of a glass support for adhesion during UV irradiation (Figure 6a, lower panel). Adhesion strength for glass substrates reached 314 ± 30.5 kPa (Figure 6b, Figure S14) with the precursor liquid prepared without NaCl and an assembly time of 1.5 h. We also note that the same mixture at the assembly time of less than 1 h tends to diffuse away from the substrates and is not deposited stably on a glass substrate (Figure S5). Overall, the trend of adhesion strength values did not show a direct correlation with the toughness data in Figure 5d. We attribute this phenomenon to the additional effect of substrate interaction with the precursor mixtures. This material showed a similar adhesion strength value when prepared and cured under seawater from

https://doi.org/10.1021/jacs.3c10528
J. Am. Chem. Soc. 2023, 145, 27022−27029

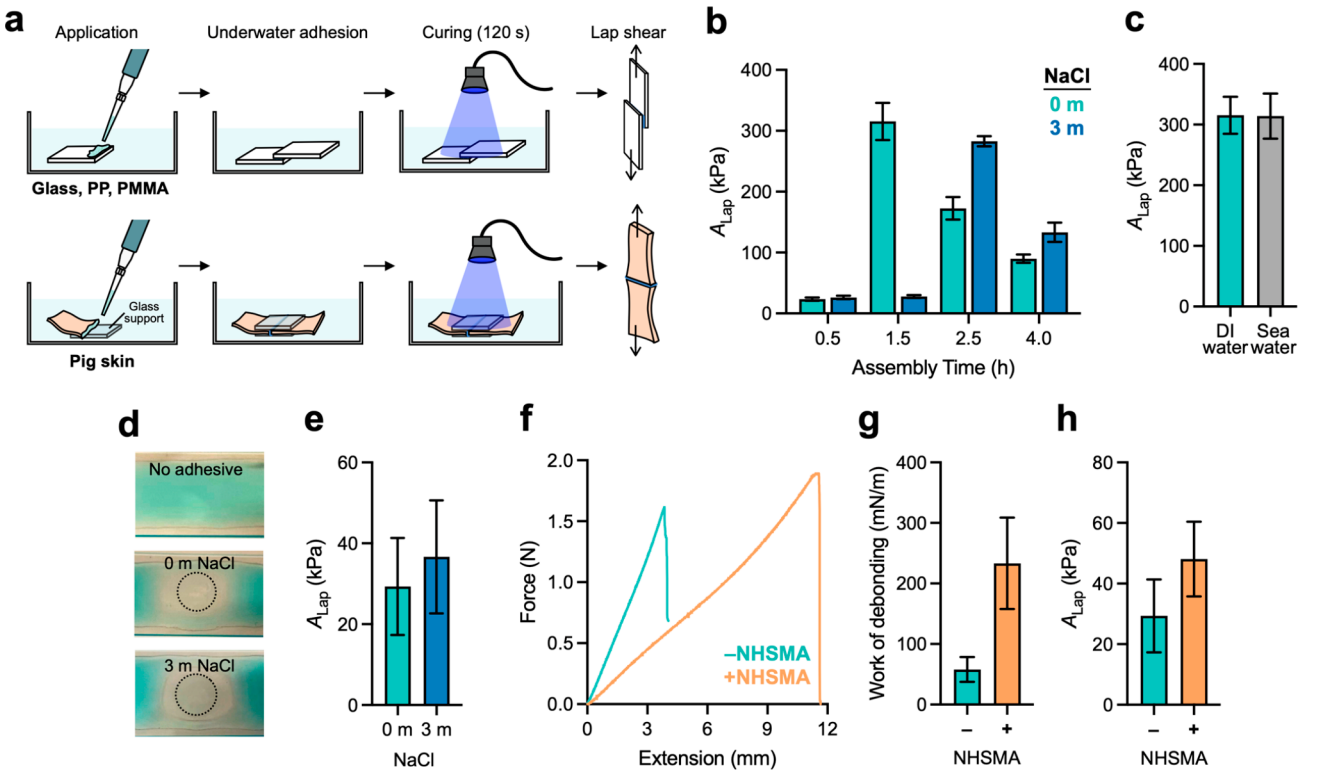

Figure 6. Tough and fast-acting underwater adhesives. (a) Schematic illustration of measuring underwater adhesion. (b) Lap shear adhesion strength values for a glass substrate with different assembly times and droplet sizes. (c) Lap shear adhesion strength values when applied and cured under distilled water and seawater. (d) Photographic images of interfacial water containing $CuSO_4$ (1 M) for visualization purposes upon applying adhesive precursors. (e) Lap shear adhesion strength values for a porcine skin substrate. (f) Force–extension curve in the absence and presence of 1% NHSMA additive measured with a porcine skin substrate. (g) Work of debonding in the absence and presence of 1% NHSMA additive measured with a porcine skin substrate. (h) Lap shear adhesion strength values in the absence and presence of 1% NHSMA additive measured with a porcine skin substrate. Error bars represent ± s.e.m. $N = 3$.

Huntington Beach, California (Figure 6c, Figures S15 and S16). We also tested PMMA and PP, and they showed adhesion values of 60 ± 3.8 and 20 ± 7.7 kPa, respectively (Figures S17–S20).

We directly observed the interaction between the precursor mixture and water on a wet glass surface to understand how these materials function as an underwater adhesive (Figure 6d, Supplementary Videos 2 and 3). As soon as the precursor mixture was applied, the surrounding interfacial water was immediately repelled, further away from the substrate–precursor boundary. Contact angle measurements also revealed that substrate–precursor interaction was stronger than substrate–water interaction in all tested substrates (Figure S24).

The adhesion value of this material with porcine skin substrates reached 37 ± 17 kPa with a precursor solution in 3 m NaCl (Figure 6e, Figures S21 and S22). Because porcine skin bears various nucleophilic functional groups on its surface, we sought to suppress adhesive failure and increase overall adhesion performance by incorporating methacrylic acid *N*-hydroxysuccinimide ester (NHSMA). Tensile testing of the adhesives containing NHSMA (1 wt % in methacrylate species) showed increased failure strain than the ones without NHSMA (Figure 6f, Figure S23). Work of debonding (WoD) of the adhesives containing NHSMA showed a 3.7-fold increase from that without NHSMA (Figure 6g). NHSMA also increased adhesion strength (Figure 6h). Therefore, adhesives with NHSMA showed increased ductility, which is important for the performance stability of adhesives by preventing sudden failures.[37]

CONCLUSIONS

We report kinetically trapped self-assembly of a compartmentalized network of liquid droplets from small-molecule precursors and its utility for a tough and fast-acting underwater adhesive. Mixtures of two small molecules, TMeOSMA and SBMA, undergo concurrent hydrolysis, condensation, and LLPS to form a viscoelastic solid via interconnected liquid droplets. Zwitterionic SBMA molecules localize on the surface of the droplet, and their molecularly interlocked structure drives the formation of the network. By photo-cross-linking the methacrylate part of the small-molecule precursors, we revealed that the hierarchical microstructure increases toughness, stretchability, and adhesion of the resulting materials. Finally, we demonstrated application of this material for tough and fast-acting underwater adhesives for various substrates.

Functional, self-assembled hierarchical structures are one of the distinguishing characteristics of biological materials. This work demonstrates relatively simple means to access complex hierarchical structures comprising liquid compartments. Distinct from prior studies in LLPS and protocell formation, our system utilizes multiple processes occurring at the same time: hydrolysis, condensation, LLPS, and self-organization of zwitterionic molecules on the droplet surface. We expect this and the following work will expand the design space for biomimetic materials.

https://doi.org/10.1021/jacs.3c10528
J. Am. Chem. Soc. 2023, 145, 27022–27029

The simplistic nature of utilizing an aqueous one-pot assembly of scalable small-molecule precursors is particularly meaningful for practical applications. Many reported synthetic underwater adhesives require elaborate macromolecular synthesis, impractical curing time, or the use of organic solvents in their formulation.[36] Our serendipitous discovery circumvents these existing challenges and will broaden the scope of adhesives for underwater repairs or emergency wound care.

■ ASSOCIATED CONTENT

Supporting Information

The Supporting Information is available free of charge at https://pubs.acs.org/doi/10.1021/jacs.3c10528.

Materials, instrumentation, experimental and synthetic methods, phase-contrast and fluorescence microscopy results, tensile testing, rheological characterization, contact angle measurement (PDF)

Visualization of N_2 bubbling setup (MOV)

Visualization of water repulsion upon applying 0 m NaCl to a wet glass substrate, as shown in Figure 6d (MOV)

Visualization of water repulsion upon applying 3 m NaCl to a wet glass substrate, as shown in Figure 6d (MOV)

■ AUTHOR INFORMATION

Corresponding Author

Seunghyun Sim − *Department of Chemistry, Department of Chemical and Biomolecular Engineering, and Department of Biomedical Engineering, University of California Irvine, Irvine, California 92697, United States; Center for Complex and Active Materials, University of California, Irvine, Irvine, California 92697, United States;* orcid.org/0000-0002-4232-5917; Email: s.sim@uci.edu

Author

Hyuna Jo − *Department of Chemistry, University of California Irvine, Irvine, California 92697, United States; Center for Complex and Active Materials, University of California, Irvine, Irvine, California 92697, United States*

Complete contact information is available at: https://pubs.acs.org/10.1021/jacs.3c10528

Author Contributions

The manuscript was written through contributions of all authors, and all authors have given approval to the final version of the manuscript.

Notes

The authors declare the following competing financial interest(s): A provisional patent based on this work has been filed.

■ ACKNOWLEDGMENTS

This work is primarily supported by the National Science Foundation Materials Research Science and Engineering Center program through the UC Irvine Center for Complex and Active Materials (DMR-2011967). The authors acknowledge support from the UC Irvine start-up fund and the use of facilities and instrumentation at the UC Irvine Materials Research Institute (IMRI) supported in part by the National Science Foundation Materials Research Science and Engineering Center program through the UC Irvine Center for Complex and Active Materials (DMR-2011967). Fourier-transform infrared spectroscopy measurements were performed at the Laser Spectroscopy Laboratories, and the nuclear magnetic resonance measurements were done in the NMR facility, both in the Department of Chemistry, University of California, Irvine. Confocal laser scanning microscopy experiments were performed at The Optical Biology Center in the School of Biological Sciences, University of California, Irvine. The authors thank the Yee lab for the use of their contact angle measurement device and Professor Kenneth J. Shea for his insightful comments.

■ REFERENCES

(1) Ingber, D. E. Tensegrity I. Cell structure and hierarchical systems biology. *Journal of cell science* **2003**, *116* (7), 1157−1173.

(2) Gao, H.; Wang, X.; Yao, H.; Gorb, S.; Arzt, E. Mechanics of hierarchical adhesion structures of geckos. *Mech. Mater.* **2005**, *37* (2−3), 275−285.

(3) Zheng, Y.; Bai, H.; Huang, Z.; Tian, X.; Nie, F.-Q.; Zhao, Y.; Zhai, J.; Jiang, L. Directional water collection on wetted spider silk. *Nature* **2010**, *463* (7281), 640−643.

(4) Yang, W.; Chen, I. H.; Gludovatz, B.; Zimmermann, E. A.; Ritchie, R. O.; Meyers, M. A. Natural flexible dermal armor. *Adv. Mater.* **2013**, *25* (1), 31−48.

(5) Brangwynne, C. P.; Eckmann, C. R.; Courson, D. S.; Rybarska, A.; Hoege, C.; Gharakhani, J.; Jülicher, F.; Hyman, A. A. Germline P granules are liquid droplets that localize by controlled dissolution/condensation. *Science* **2009**, *324* (5935), 1729−1732.

(6) Quiroz, F. G.; Fiore, V. F.; Levorse, J.; Polak, L.; Wong, E.; Pasolli, H. A.; Fuchs, E. Liquid-liquid phase separation drives skin barrier formation. *Science* **2020**, *367* (6483), No. eaax9554.

(7) Alberti, S.; Gladfelter, A.; Mittag, T. Considerations and challenges in studying liquid-liquid phase separation and biomolecular condensates. *Cell* **2019**, *176* (3), 419−434.

(8) Hyman, A. A.; Weber, C. A.; Jülicher, F. Liquid-liquid phase separation in biology. *Annual review of cell and developmental biology* **2014**, *30*, 39−58.

(9) Gao, N.; Mann, S. Membranized coacervate microdroplets: from versatile protocell models to cytomimetic materials. *Acc. Chem. Res.* **2023**, *56* (3), 297−307.

(10) Mason, A. F.; Buddingh', B. C.; Williams, D. S.; Van Hest, J. C. Hierarchical self-assembly of a copolymer-stabilized coacervate protocell. *J. Am. Chem. Soc.* **2017**, *139* (48), 17309−17312.

(11) Gao, N.; Xu, C.; Yin, Z.; Li, M.; Mann, S. Triggerable protocell capture in nanoparticle-caged coacervate microdroplets. *J. Am. Chem. Soc.* **2022**, *144* (9), 3855−3862.

(12) Zhang, Y.; Wang, Z.; Li, M.; Xu, C.; Gao, N.; Yin, Z.; Wang, K.; Mann, S.; Liu, J. Osmotic-Induced Reconfiguration and Activation in Membranized Coacervate-Based Protocells. *J. Am. Chem. Soc.* **2023**, *145* (18), 10396−10403.

(13) Ji, Y.; Lin, Y.; Qiao, Y. Plant Cell-Inspired Membranization of Coacervate Protocells with a Structured Polysaccharide Layer. *J. Am. Chem. Soc.* **2023**, *145* (23), 12576−12585.

(14) Liu, J.; Tian, L.; Qiao, Y.; Zhou, S.; Patil, A. J.; Wang, K.; Li, M.; Mann, S. Hydrogel-immobilized coacervate droplets as modular microreactor assemblies. *Angew. Chem., Int. Ed.* **2020**, *59* (17), 6853−6859.

(15) Downs, F. G.; Lunn, D. J.; Booth, M. J.; Sauer, J. B.; Ramsay, W. J.; Klemperer, R. G.; Hawker, C. J.; Bayley, H. Multi-responsive hydrogel structures from patterned droplet networks. *Nature Chem.* **2020**, *12* (4), 363−371.

(16) Lee, M. N.; Mohraz, A. Bicontinuous macroporous materials from bijel templates. *Adv. Mater.* **2010**, *22* (43), 4836−4841.

(17) Perelaer, J.; Smith, P. J.; Hendriks, C. E.; van den Berg, A. M.; Schubert, U. S. The preferential deposition of silica micro-particles at the boundary of inkjet printed droplets. *Soft Matter* **2008**, *4* (5), 1072−1078.

(18) Shao, Q.; Jiang, S. Molecular understanding and design of zwitterionic materials. *Adv. Mater.* **2015**, *27* (1), 15−26.

(19) Dong, D.; Tsao, C.; Hung, H.-C.; Yao, F.; Tang, C.; Niu, L.; Ma, J.; MacArthur, J.; Sinclair, A.; Wu, K.; et al. High-strength and fibrous capsule−resistant zwitterionic elastomers. *Science Advances* **2021**, *7* (1), No. eabc5442.
(20) Shao, Q.; Mi, L.; Han, X.; Bai, T.; Liu, S.; Li, Y.; Jiang, S. Differences in cationic and anionic charge densities dictate zwitterionic associations and stimuli responses. *J. Phys. Chem. B* **2014**, *118* (24), 6956−6962.
(21) Chen, X.; Eldred, D.; Liu, J.; Chiang, H.; Wang, X.; Rickard, M. A.; Tu, S.; Cui, L.; LaBeaume, P.; Skinner, K. Simultaneous in situ monitoring of trimethoxysilane hydrolysis reactions using Raman, infrared, and nuclear magnetic resonance (NMR) spectroscopy aided by chemometrics and Ab Initio calculations. *Appl. Spectrosc.* **2018**, *72* (9), 1404−1415.
(22) Nam, K.-H.; Lee, T.-H.; Bae, B.-S.; Popall, M. Condensation reaction of 3-(methacryloxypropyl)-trimethoxysilane and diisobutylsilanediol in non-hydrolytic sol-gel process. *J. Sol-Gel Sci. Technol.* **2006**, *39*, 255−260.
(23) Sepeur, S.; Kunze, N.; Werner, B.; Schmidt, H. UV curable hard coatings on plastics. *Thin Solid Films* **1999**, *351* (1−2), 216−219.
(24) Ado, G.; Noda, N.; Vu, H. T.; Perron, A.; Mahapatra, A. D.; Arista, K. P.; Yoshimura, H.; Packwood, D. M.; Ishidate, F.; Sato, S.-i.; et al. Discovery of a phase-separating small molecule that selectively sequesters tubulin in cells. *Chemical Science* **2022**, *13* (19), 5760−5766.
(25) Huang, Y.; Wang, X.; Li, J.; Lin, Y.; Chen, H.; Liu, X.; Huang, X. Reversible Light-Responsive Coacervate Microdroplets with Rapid Regulation of Enzymatic Reaction Rate. *ChemSystemsChem.* **2021**, *3* (5), No. e2100006.
(26) Kitamura, A.; Kinjo, M. Determination of diffusion coefficients in live cells using fluorescence recovery after photobleaching with wide-field fluorescence microscopy. *Biophysics and Physicobiology* **2018**, *15*, 1−7.
(27) Priftis, D.; Tirrell, M. Phase behaviour and complex coacervation of aqueous polypeptide solutions. *Soft Matter* **2012**, *8* (36), 9396−9405.
(28) Priftis, D.; Xia, X.; Margossian, K. O.; Perry, S. L.; Leon, L.; Qin, J.; de Pablo, J. J.; Tirrell, M. Ternary, tunable polyelectrolyte complex fluids driven by complex coacervation. *Macromolecules* **2014**, *47* (9), 3076−3085.
(29) Neitzel, A. E.; Fang, Y. N.; Yu, B.; Rumyantsev, A. M.; de Pablo, J. J.; Tirrell, M. V. Polyelectrolyte complex coacervation across a broad range of charge densities. *Macromolecules* **2021**, *54* (14), 6878−6890.
(30) Scognamiglio, F.; Travan, A.; Rustighi, I.; Tarchi, P.; Palmisano, S.; Marsich, E.; Borgogna, M.; Donati, I.; de Manzini, N.; Paoletti, S. Adhesive and sealant interfaces for general surgery applications. *Journal of Biomedical Materials Research Part B: Applied Biomaterials* **2016**, *104* (3), 626−639.
(31) Jaiswal, P. R.; Kumar, R. I.; Juwet, T.; Luyckx, G.; Verhaeghe, C.; De Waele, W. Experimental deformation analysis of an adhesively bonded multi-material joint for marine applications. *Strain* **2023**, *59* (2), No. e12433.
(32) Tan, K. T.; Vogt, B. D.; White, C. C.; Steffens, K. L.; Goldman, J.; Satija, S. K.; Clerici, C.; Hunston, D. L. On the origins of sudden adhesion loss at a critical relative humidity: examination of bulk and interfacial contributions. *Langmuir* **2008**, *24* (17), 9189−9193.
(33) White, C.; Tan, K. T.; Hunston, D.; Steffens, K.; Stanley, D. L.; Satija, S. K.; Akgun, B.; Vogt, B. D. Mechanisms of criticality in environmental adhesion loss. *Soft Matter* **2015**, *11* (20), 3994−4001.
(34) Maier, G. P.; Rapp, M. V.; Waite, J. H.; Israelachvili, J. N.; Butler, A. Adaptive synergy between catechol and lysine promotes wet adhesion by surface salt displacement. *Science* **2015**, *349* (6248), 628−632.
(35) Fan, H.; Gong, J. P. Bioinspired underwater adhesives. *Adv. Mater.* **2021**, *33* (44), No. 2102983.
(36) Narayanan, A.; Dhinojwala, A.; Joy, A. Design principles for creating synthetic underwater adhesives. *Chem. Soc. Rev.* **2021**, *50* (23), 13321−13345.
(37) Mazzotta, M. G.; Putnam, A. A.; North, M. A.; Wilker, J. J. Weak bonds in a biomimetic adhesive enhance toughness and performance. *J. Am. Chem. Soc.* **2020**, *142* (10), 4762−4768.

https://doi.org/10.1021/jacs.3c10528
J. Am. Chem. Soc. 2023, 145, 27022−27029